J. Fluid Mech. (1982), *vol.* 122, *pp.* 369–394
Printed in Great Britain

The effect of the upstream boundary-layer state on the shock interaction at a compression corner

By KIYOTAKA HAYAKAWA† AND L. C. SQUIRE
Cambridge University Engineering Department, Trumpington Street, Cambridge

(Received 4 August 1980 and in revised form 18 March 1982)

In most experimental studies of the shock-wave/boundary-layer interaction at a compression corner the boundary layer upstream of the interaction has developed in zero-pressure-gradient conditions. However, in many practical situations the boundary layer upstream of the interaction is subject to adverse or favourable pressure gradients, and hence is in a non-equilibrium state. This paper presents the results of a series of experiments on the interaction at a compression corner where the boundary layer upstream of the corner is disturbed by air injected through a porous surface. The results are thus of direct interest to the design of transpiration-cooled aerodynamic surfaces. However, the boundary-layer profiles upstream of the interaction also have many similarities to those in an adverse pressure gradient, so that the results also give some indication of the effects of an isentropic compression upstream of the interaction. The results are used to discuss existing correlations for upstream influence and to study conditions for incipient separation. The experiments were made at Mach numbers of 1·8, 2·5, 2·7 and 2·9, with corner angles of 8°, 10°, 12°, 13° and 14°.

1. Introduction

The development of supersonic and hypersonic flight, together with advances in turbomachinery, has produced the need for a complete understanding of the interactions between shock waves and boundary layers, and numerous experimental and theoretical investigations of these interactions have been made, particularly of flows with separation.

So far this research has yielded a fairly good qualitative insight into the structure of the interaction. However, our understanding is still far from complete regarding the basic mechanism of flow separation at the interaction, particularly the conditions under which separation first occurs (incipient separation) and the complex effects of Reynolds number and Mach number on incipient separation. Also, the majority of previous studies concern the interaction of a shock wave with an equilibrium boundary layer that has developed in a zero-pressure gradient. Although further investigations are necessary on this type of interaction, most practical problems involve far more complicated boundary layers. For example, on a transonic aerofoil the boundary layer may undergo either a favourable or an adverse pressure gradient before it meets a normal shock wave. A similar situation could be encountered at the hinge of a deflected control. It is therefore important, from a practical point of view, to understand the effect of the upstream boundary-layer state on the shock-wave interaction.

† Present address: Gas Dynamics Laboratory, Princeton University, U.S.A.

Squire & Smith (1980) conducted a series of experiments to investigate the influence of the shape of the upstream boundary layer on the shock strength required to induce separation at Mach numbers of 1·8 and 2·5. The interaction was produced on a flat plate by an incident oblique shock wave of varying strength, and an air-injection apparatus was used to alter the shape of the upstream boundary layer. By injecting air through a porous plate and by changing the injection rate, the fullness of the boundary layer profile can easily be reduced. This results in a decrease in skin-friction coefficient and an increase in the shape factor of the boundary layer; this is similar to the situation experienced in an adverse pressure gradient. Modifying the boundary-layer shape in this manner has an advantage over creating an adverse pressure gradient by varying the wall curvature in that the tunnel blockage problem can be minimized. It should, however, be noted that the shock interaction took place on a solid plate situated downstream of the porous plate where the boundary layer disturbed by the injection was recovering under zero pressure gradient.

One surprising result obtained by Squire & Smith (1980) was that the shock strength to produce incipient separation was virtually independent of the shape of the upstream boundary layer. It had been thought intuitively that the presence of an adverse pressure gradient or transpiration upstream of the interaction would promote earlier separation. The scale of interaction and the growth of the separated region, on the other hand, were found to increase rapidly with increasing injection rate. Squire & Smith's results suffered, unfortunately, from the effect of three-dimensionality, mainly due to the incident oblique shock wave interacting with the boundary layers on the sidewalls of the tunnel. In order to overcome this problem a series of compression corners of different inclinations were used in the present investigation.

2. Details of the experiments

The experiments were performed in an intermittent supersonic wind tunnel at the Engineering Department of the University of Cambridge as shown in figure 1. It was essentially the same as that used by Squire & Smith (1980) except that the incident shock generator was removed and the solid flat plate was replaced by a compression-corner model. Upstream of the model there was a porous plate, through which air was injected at a controlled rate to deform the boundary layer.

The experiments were conducted at Mach numbers of 1·8, 2·5, 2·7 and 2·9, and the corresponding Reynolds numbers per metre were $3{\cdot}8\times10^7$, $3{\cdot}8\times10^7$, $4{\cdot}0\times10^7$ and $4{\cdot}1\times10^7$. For each Mach number, six injection rates, including zero, were used for corner angles of 8°, 10°, 12°, 13° and 14°. The six injection rates are referred to here as $FP = 0, 1, 2, 3, 4$ and 5, where zero corresponds to no injection and five to the highest injection rate used. The actual injection rates $\rho_w V_w/\rho_e U_e$, are shown in table 1.

The main tests included measurements of static pressure distributions, and in the absence of a shock wave (i.e. in the absence of a compression corner), pitot traverses through the boundary layer and measurements of skin friction by a Preston tube. The flow was also studied using schlieren and shadowgraph photography and two types of oil-flow visualization. The first was the conventional method using a mixture of titanium dioxide, oil and oleic acid to act as a dispersing agent (Maltby 1962). The second method was an oil-bleed method devised by Smith (1977), in which a mixture of oil and chemical solvent was bled into the tunnel through a pressure hole upstream

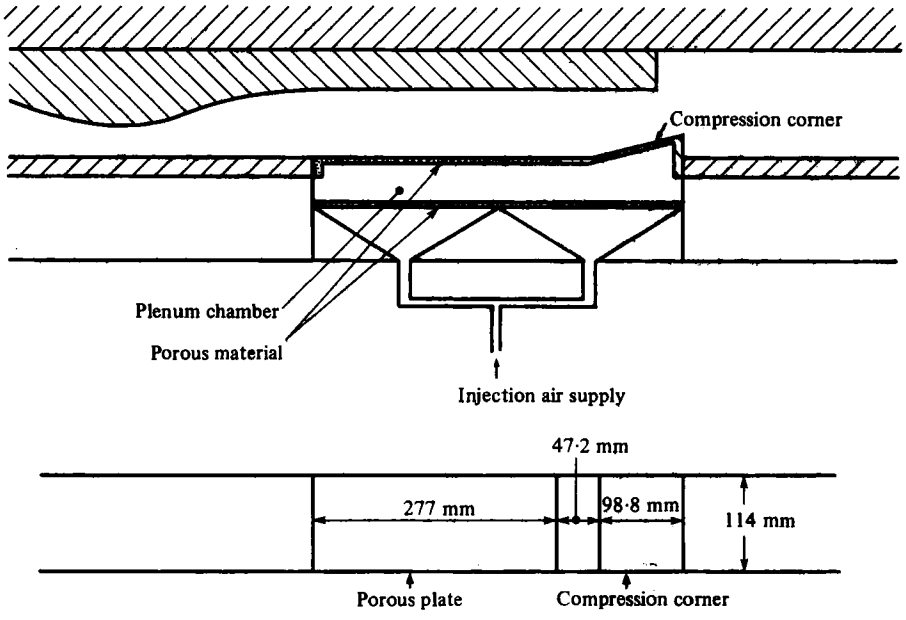

FIGURE 1. Cross-sectional view of the working section.

FP \ *M*	1·8	2·5	2·7	2·9
0	0	0	0	0
1	0·0006	0·0009	0·0008	0·0009
2	0·0012	0·0016	0·0016	0·0017
3	0·0017	0·0024	0·0023	0·0025
4	0·0022	0·0031	0·0030	0·0032
5	0·0027	0·0038	0·0036	0·0039

TABLE 1. Actual injection rates $\rho_w V_w/\rho_e U_e$, corresponding to the values of the injection parameter, FP

of the interaction. Once on the surface the solvent evaporated leaving a mobile oil film on the surface.

In order to measure boundary-layer profiles upstream of the corner in the absence of the shock, the test surface was replaced by a flat surface and a traverse system was mounted downstream. This traverse system could be used to traverse the boundary layer with a variety of probes including a flattened Pitot tube for boundary-layer profiles and a circular Preston tube for measurement of skin friction (using the Bradshaw & Unsworth (1973) calibration). The temperature profile through the layer was not measured. Instead it was assumed that the temperature was related to the velocity by the relation

$$T = T_w + (T_r - T_w)\left(\frac{u}{U_e}\right) - (T_r - T_e)\left(\frac{u}{U_e}\right)^2, \tag{1}$$

where T_w is the measured wall temperature, T_e is the free-stream static temperature calculated from the tunnel stagnation temperature, and T_r is the recovery temperature.

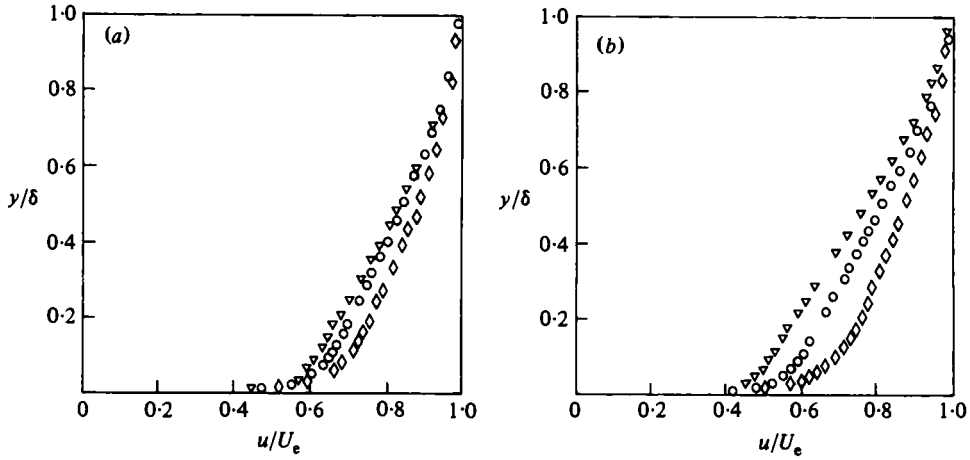

FIGURE 2. Velocity profiles of incoming boundary layers at $X = 47{\cdot}2$ mm. (a) $M = 1{\cdot}8$, (b) $M = 2{\cdot}5$. ◇, $FP = 0$; ○, $FP = 3$; ▽, $FP = 5$.

During the 60 s tunnel run the stagnation temperature rose by about 5 °C while the wall temperature fell by about the same amount, so that the ratio T_w/T_r varied between 1·05 and 1·01 during the run. Instantaneous values of T_w, T_r, and T_e were used in (1), and the accuracy of the approach is fully discussed by Chew & Squire (1979).

3. Basic results

3.1. *Upstream boundary-layer state*

Typical results of the boundary-layer development measured in the absence of a shock wave (i.e. in the absence of a compression corner) at the six injection rates at $M = 1{\cdot}8$, 2·5, 2·7 and 2·9 are presented in figures 2–6. Emphasis is placed on the effect of injection on the various boundary-layer parameters at $x = 47{\cdot}2$ mm, where the compression corner is to be installed.

The velocity profiles for sample injection rates measured at 47·2 mm downstream of the porous–solid-plate junction (i.e. the position of the compression corner) are plotted as u/U_e against y/δ in figure 2 for Mach number of 1·8 and 2·5. As can be seen, the profiles tend to become less full with increase in injection rate and suggest a stronger wake component with increasing injection rate. Figure 3 shows the variation of the boundary-layer thickness ($u/U_e = 0{\cdot}995$) in the streamwise direction for all the injection rates. The thickening of the boundary layer as a result of the increased injection can clearly be seen.

In order to show the variation of boundary-layer shape along the surface the incompressible shape factors H_1 are presented in figure 4;

$$H_1 = \int_0^\delta \left(1 - \frac{u}{U_e}\right) dy \Big/ \int_0^\delta \left(1 - \frac{u}{U_e}\right) \frac{u}{U_e} dy.$$

This factor, rather than the true shape factor H, was chosen because H is strongly dependent on Mach number, and hence it is difficult to compare results at different Mach numbers. As will be seen the boundary layer is relaxing along the plate with H_1

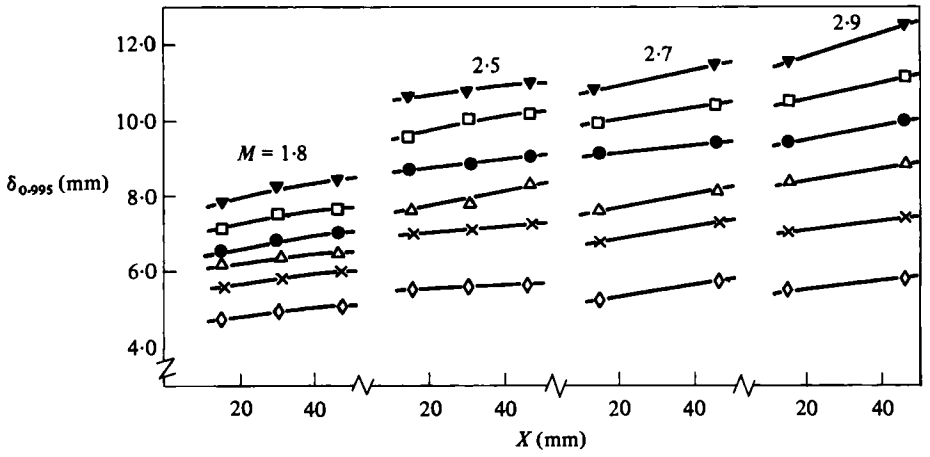

FIGURE 3. Boundary-layer-thickness distributions of incoming boundary layers. ◇, FP = 0; ×, 1; △, 2; ●, 3; □, 4; ▼, 5.

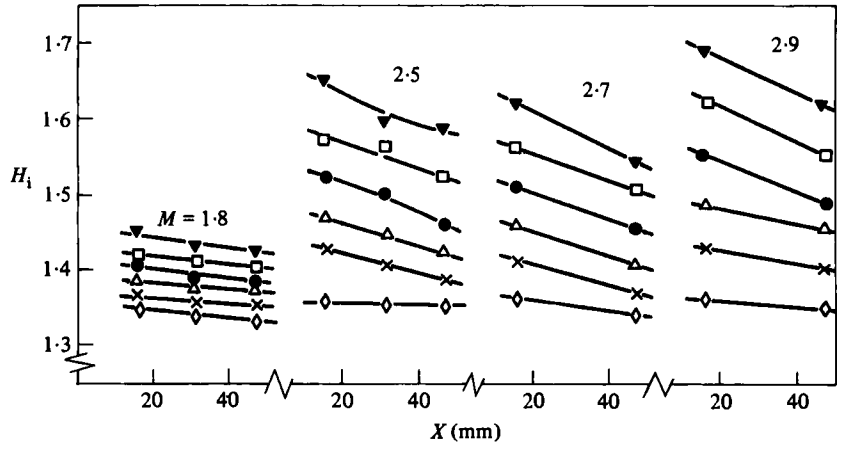

FIGURE 4. Incompressible shape factors of incoming boundary layers. Key as in figure 3.

slowly falling from the high values that occur at the end of the region of injection. In the absence of injection H_i is close to 1·35 at all Mach numbers, and with injection H_i has values of about 1·6 at the position of the compression corner with the highest injection rates at the higher Mach numbers. The significance of this increase in H_i in terms of an equivalent adverse pressure gradient is discussed fully by Squire & Smith (1980). Here it is sufficient to point out that in one experimental study where the freestream Mach number fell from 4·0 to 2·0 in about 40 boundary-layer thicknesses the measured increase in H_i was about 0·15 above the value of H_i in a constant-Mach-number stream at 4·0.

The corresponding variations in skin-friction coefficient are shown in figure 5. As can be seen, there is a dramatic reduction in skin friction immediately downstream of the porous surface with injection. However, downstream of the porous surface the skin friction increases before reaching a fairly constant level in the region where the compression corner is to be installed (X = 47·2 mm). The reduction in skin-friction

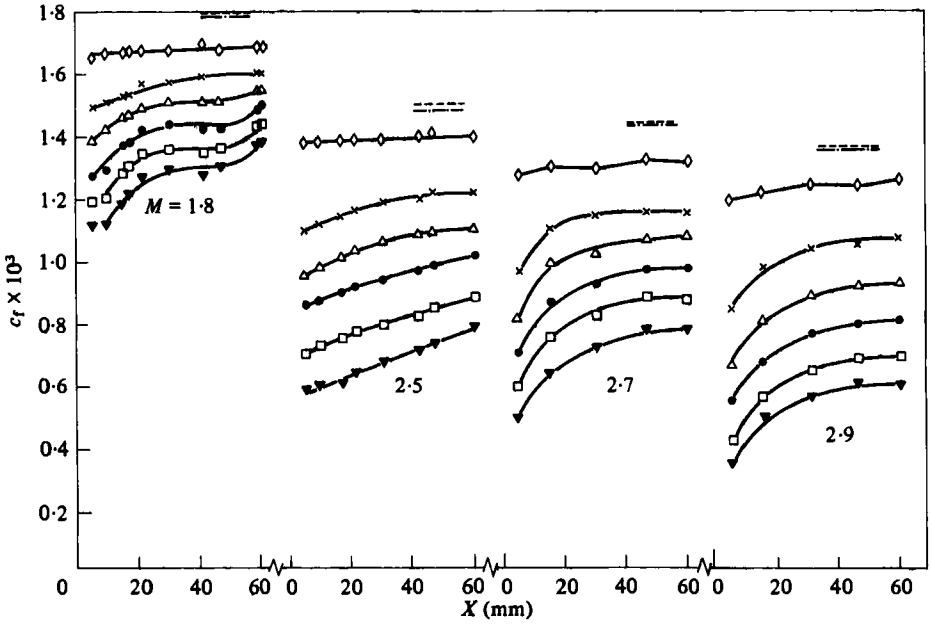

FIGURE 5. Skin-friction coefficients of the incoming boundary layer. —·—, Spalding & Chi (1964); – – – –, Winter & Gaudet (1970). Experimental points as in figure 3.

coefficient achieved at $X = 47{\cdot}2$ mm by the highest injection rate at $M = 1{\cdot}8$ is approximately 25% and at $M = 2{\cdot}5$, 2·7 and 2·9 is 45 to 50% of the values without injection.

The chain line and the broken line shown in figure 5 indicate the skin-friction coefficients obtained respectively from the skin-friction coefficient formulae of Spalding & Chi (1964) and Winter & Gaudet (1970) at $X = 47{\cdot}2$ mm without injection. The present data are seen to lie near the lower limit of their claimed accuracy.

Figure 6 shows the velocity profiles at $X = 16$ mm plotted in law-of-the-wall co-ordinates, using a transformation to incompressible flow based on mixing length as suggested by van Driest (1951). In all cases the measured values in the inner region are in excellent agreement with the incompressible law of the wall. It will also be seen that the decrease in fullness of the velocity profiles is reflected in an increase in the wake component that resembles that in an adverse pressure gradient. The stronger wake component with increasing injection rate is, however, due entirely to the upstream effect of the injection, since the local pressure gradients are small.

In the absence of injection the momentum thickness just ahead of the corner position is about 0·5 mm, so the Reynolds number based on momentum thickness is close to 20000, which indicates that the boundary layer is completely turbulent in all conditions. In fact, early investigations by Jeromin (1966) in the same tunnel showed that the boundary layer was fully turbulent at positions well ahead of the porous plate.

3.2. *Two-dimensionality*

Before proceeding any further, it should be recalled that the earlier tests by Squire & Smith (1980) showed considerable signs of three-dimensional flow, and it was suggested that this three-dimensionality was associated with the interaction between the

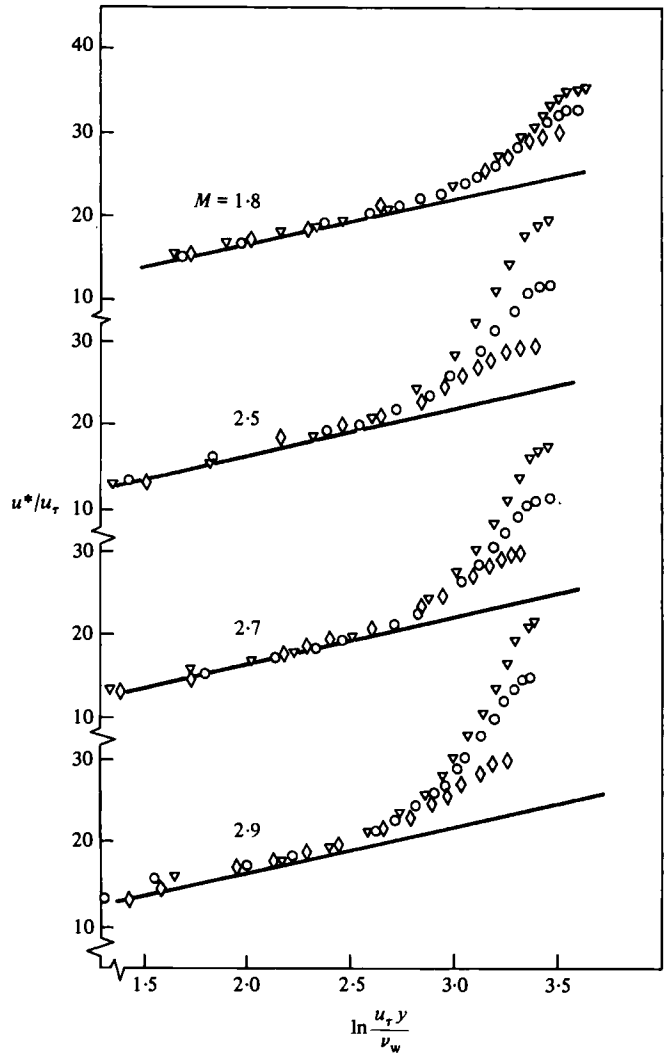

FIGURE 6. Law-of-the-wall plots at X = 16 mm. ◇, FP = 0; ○, 3; ▽, 5.

incident shock and the sidewall boundary layers. In particular, the centreline pressure distributions showed a clear hump in the interaction region, but this hump was absent in the pressure distributions measured off the centreline. Figure 7 shows the corresponding results obtained in the present study at M = 2·5 with zero injection. It will be seen that there is no sign of a hump in the pressure distributions and that the results on and off the centreline are virtually identical. Similar results were obtained with injection.

The results of the oil-flow visualization (see below; figure 14) also indicate that the flow is two-dimensional. The streaklines run parallel to one another all through the interaction. The separation lines, when present, are straight over most of the model span and normal to the flow direction. There are signs of three-dimensional effects very near the sidewalls, where, as opposed to the incident-shock interaction, the streaklines appear to be deflected away from the tunnel centreline after passing

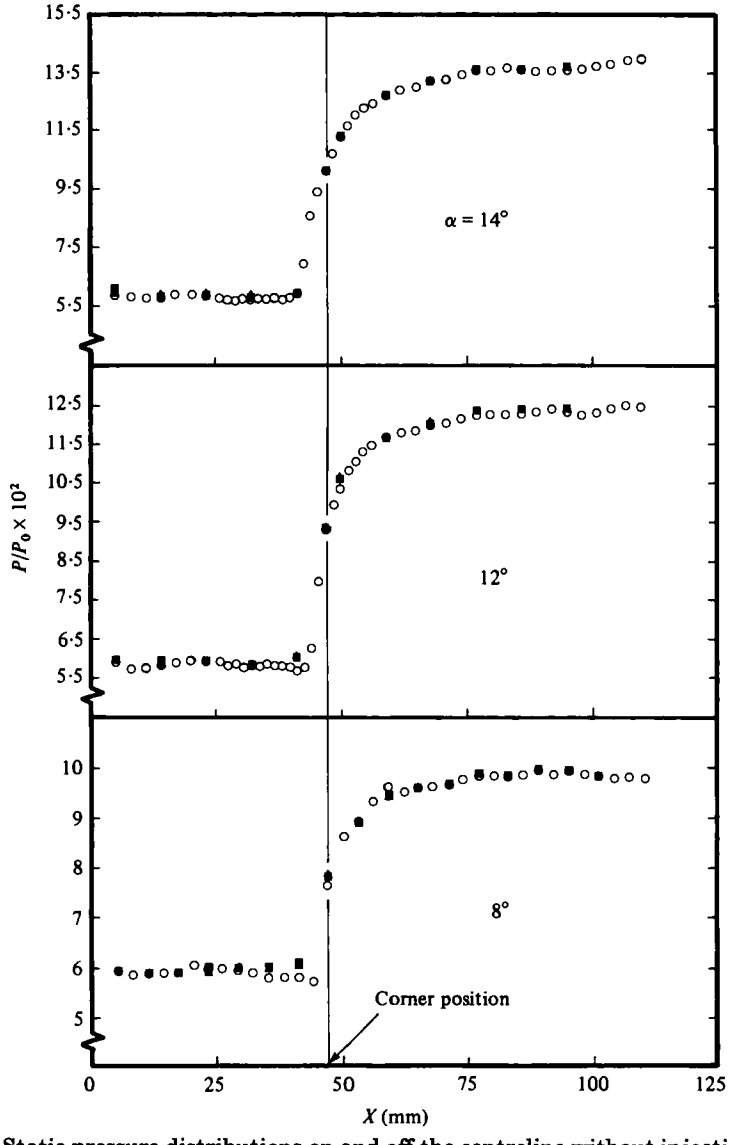

FIGURE 7. Static pressure distributions on and off the centreline without injection. ○, centreline; ▲, 20 mm off centreline (right-hand side); ■, 20 mm off centreline (left-hand side).

through the shock wave. However, these regions are confined to a small portion of the model span (approximately 7 % of the model span) and are considered to give negligible effects on the shock-wave interaction that takes place over the major part of the model span.

It can therefore be concluded that in the shock-wave interaction at the compression corners used for the present experiments the two-dimensionality of the flow is satisfactory.

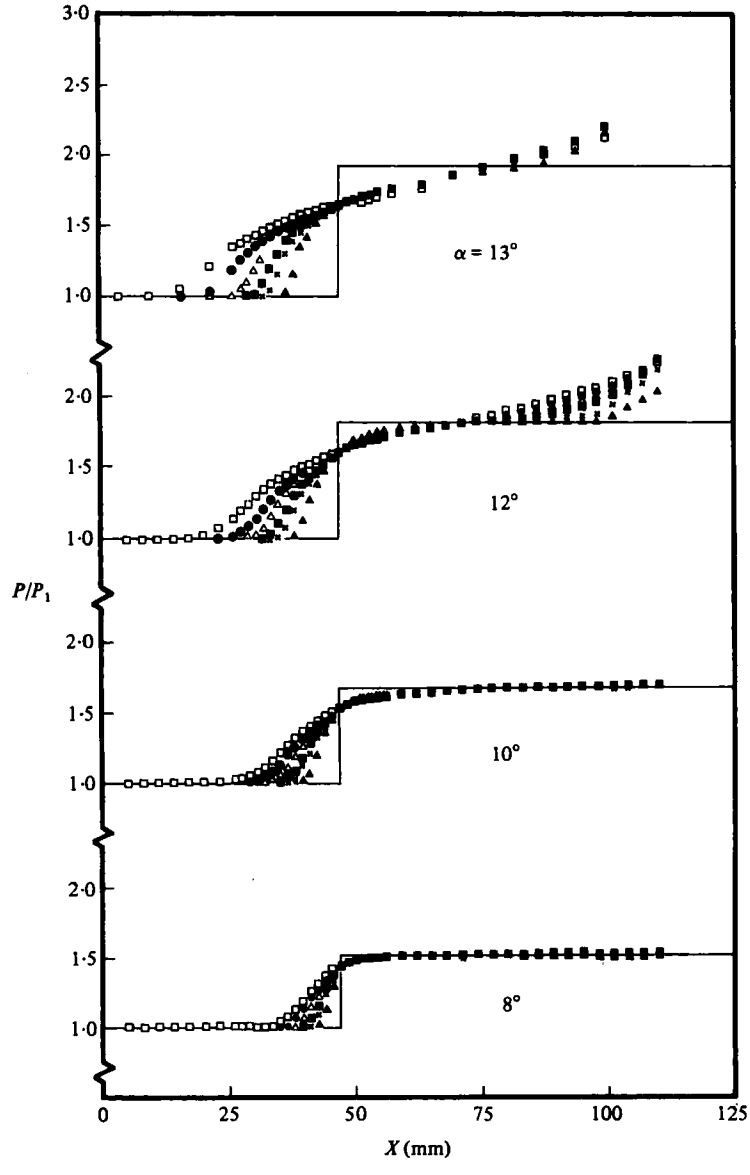

FIGURE 8. Static pressure distributions at $M = 1{\cdot}8$. ▲, $FP = 0$; ×, 1; ■, 2; △, 3; ●, 4; □, 5; ——, inviscid pressure distribution.

3.3. *Static pressure distributions*

Typical static pressure distributions through the shock interaction for two of the four Mach numbers investigated are shown in figures 8 and 9. The pressure is normalized by the pressure P_1 upstream of interaction. The results for the six injection rates, including zero injection, are plotted together at each corner angle. The distributions downstream of the corner at $\alpha = 13°$ may be unreliable, since this corner was made by machining off the ramp face of the 14° corner. It should also be noted that the results for the corner angle of 14° at a Mach number of 1·8 are not included since the

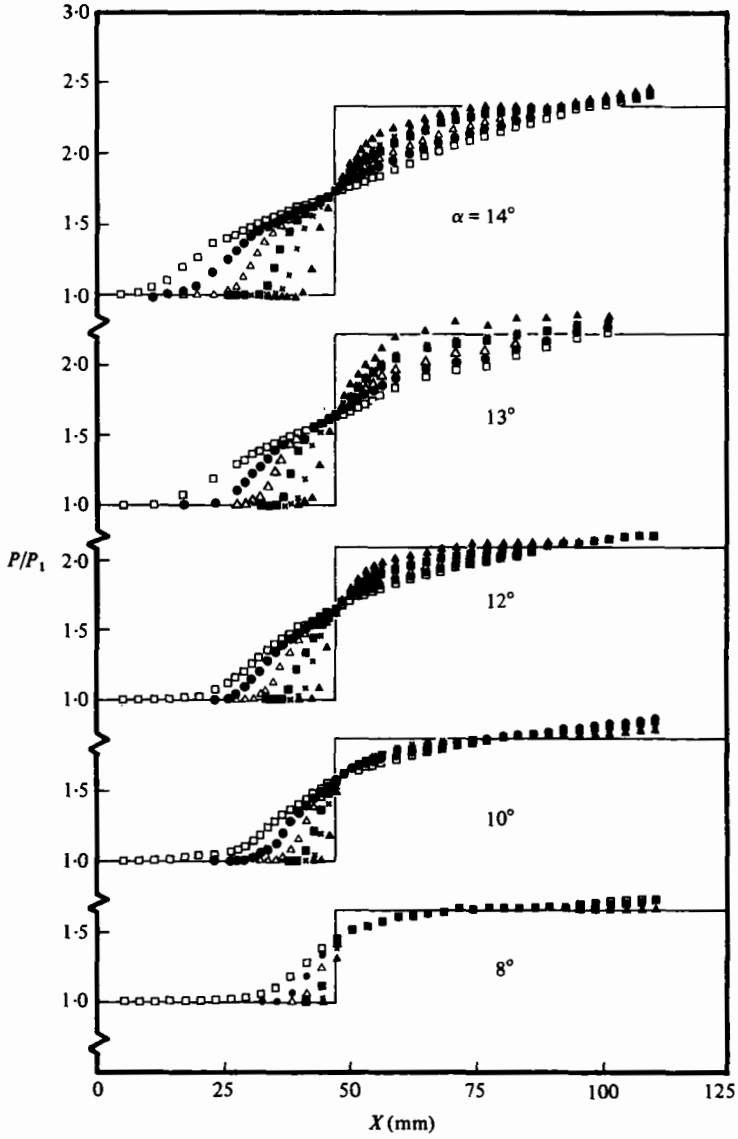

FIGURE 9. Static pressure distributions at $M = 2{\cdot}5$. Key as in figure 8.

tunnel did not start completely in this condition. In figures 8 and 9 the pressure rise in inviscid flow is indicated by the solid line. It can be seen from the figures that under all conditions the pressure starts to rise upstream of the corner. This upstream spread of pressure, normally termed 'upstream influence', increases with increasing injection rate and corner angle. This is true at all the Mach numbers investigated. In general, increasing the corner angle from the lowest to the highest angle causes a three- to fourfold increase in upstream influence. Similarly, with the highest injection rate used an approximately fourfold increase in upstream influence is achieved as compared with the zero injection case. With the highest injection rate at $\alpha = 13°$ and $14°$ at $M = 2{\cdot}9$ the pressure starts to rise upstream of the

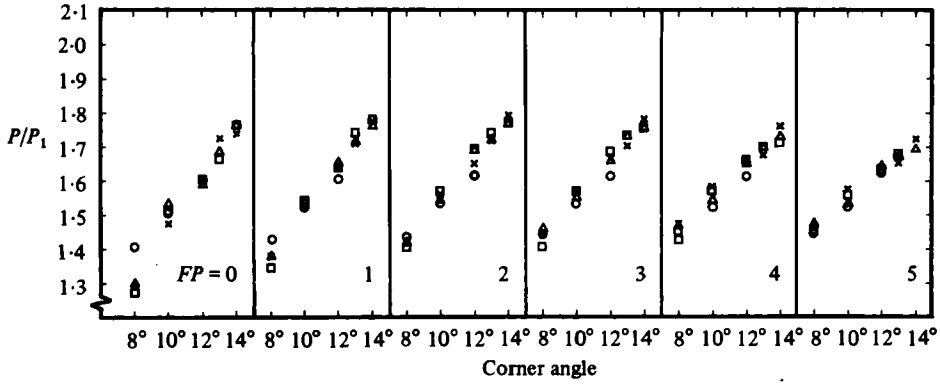

FIGURE 10. Variation of pressure at corner with corner angle. ○, M = 1·8; ×, 2·5; △, 2·7; □, 2·9.

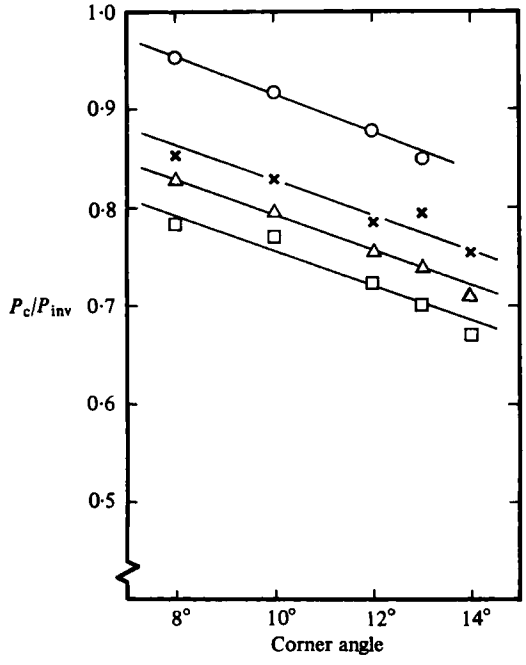

FIGURE 11. Ratio of measured pressure rise at corner to inviscid pressure rise. Key as in figure 10.

porous–solid-plate junction. The behaviour of the upstream influence will be discussed in detail in §4.

At each corner angle, except at $\alpha = 8°$, the corner pressure is almost independent of the injection rate, and when the measured corner pressures at all Mach numbers are plotted together (figure 10), it is seen that they do not depend on the Mach number. This may be coincidental, but is an interesting phenomenon. Figure 11 shows the ratio of the corner pressure achieved in the experiments to the pressure that would be reached if the flow were inviscid. The corner pressures shown are the average of the six injection rates. It is seen that although the ratio P_c/P_{inv} decreases with increasing

Mach number, it decreases roughly linearly with increasing corner angle at each Mach number.

A constant pressure level, which is close to the inviscid pressure rise for each corner angle, is reached downstream of the corner at zero injection. At all the corner angles at $M = 1{\cdot}8$ and at the smaller angles at $M = 2{\cdot}5$ the pressure distributions downstream of the corner are not much influenced by the effect of injection, and they all take a similar shape after the corner, irrespective of the injection rate. At $M = 1{\cdot}8$ with $\alpha = 12°$ the pressure increases after reaching the inviscid level. This increase is due to the impingement of the extraneous wave issuing from the junction between the end of the supersonic liner and the wooden block attached behind it on the downstream side of the corner. This liner configuration had to be used to avoid the tunnel blockage. The effect of this wave, however, is confined to far downstream of the corner and can be considered negligible for the analysis of the upstream influence to be discussed in §4. Under other conditions the pressure distributions become less convex with increasing injection, and at the higher injection rates the pressure does not become constant within the measuring region, although other tests have shown that the pressure does tend to a constant level by the end of the wedge. The wedge was made as long as possible consistent with the establishment of satisfactory flow in the tunnel, and its length is more than 8 times the thickness of the thickest incoming boundary layer ($FP = 5$, $M = 2{\cdot}9$). The work of Hunter & Reeves (1971) suggests that this length is sufficient to prevent any upstream influence from the trailing edge of the wedge, even when separation is present. In fact a series of tests at $M = 2{\cdot}5$ with a wedge angle of 13° showed that the pressure distribution and upstream influence was unchanged as the length of the wedge was reduced from 100 to 50 mm, so the results shown in figures 8 and 9 should be free of interference effects.

3.4. *Schlieren and shadowgraph photography*

A large number of schlieren and shadowgraph photographs were taken during the experiment, and some selected photographs are shown in figures 12 and 13. The location of the junction between the porous and solid plates is marked by an arrow in the first photograph of figure 13; in all cases a wave can be seen to originate from the junction. The effect of this wave on the flow downstream of the junction is considered to be minimal, since the static pressure measured at 5·5 mm downstream of the junction showed no appreciable difference from the pressure measured further downstream. This is probably due to the neutralization effect of the expansion and compression waves. The expansion waves are produced by the sudden decrease in the rate of growth of the boundary-layer thickness as a result of the cessation of injection.

With no injection present, the shock wave appears to emanate at or very near the corner position and is very thin in the photographs, suggesting that the flow compression takes place over a very short distance. With increasing injection rate and/or corner angle, the shock wave is seen to move further upstream, resulting in an increase in upstream influence.

Within the boundary layer, the shock wave or compression waves are seen to be generated very near the wall and they are nearly normal to the surface near the wall, owing to the Mach-number gradient in the boundary layer. It is also seen that at the higher injection rates they are standing at larger angles over a considerable portion

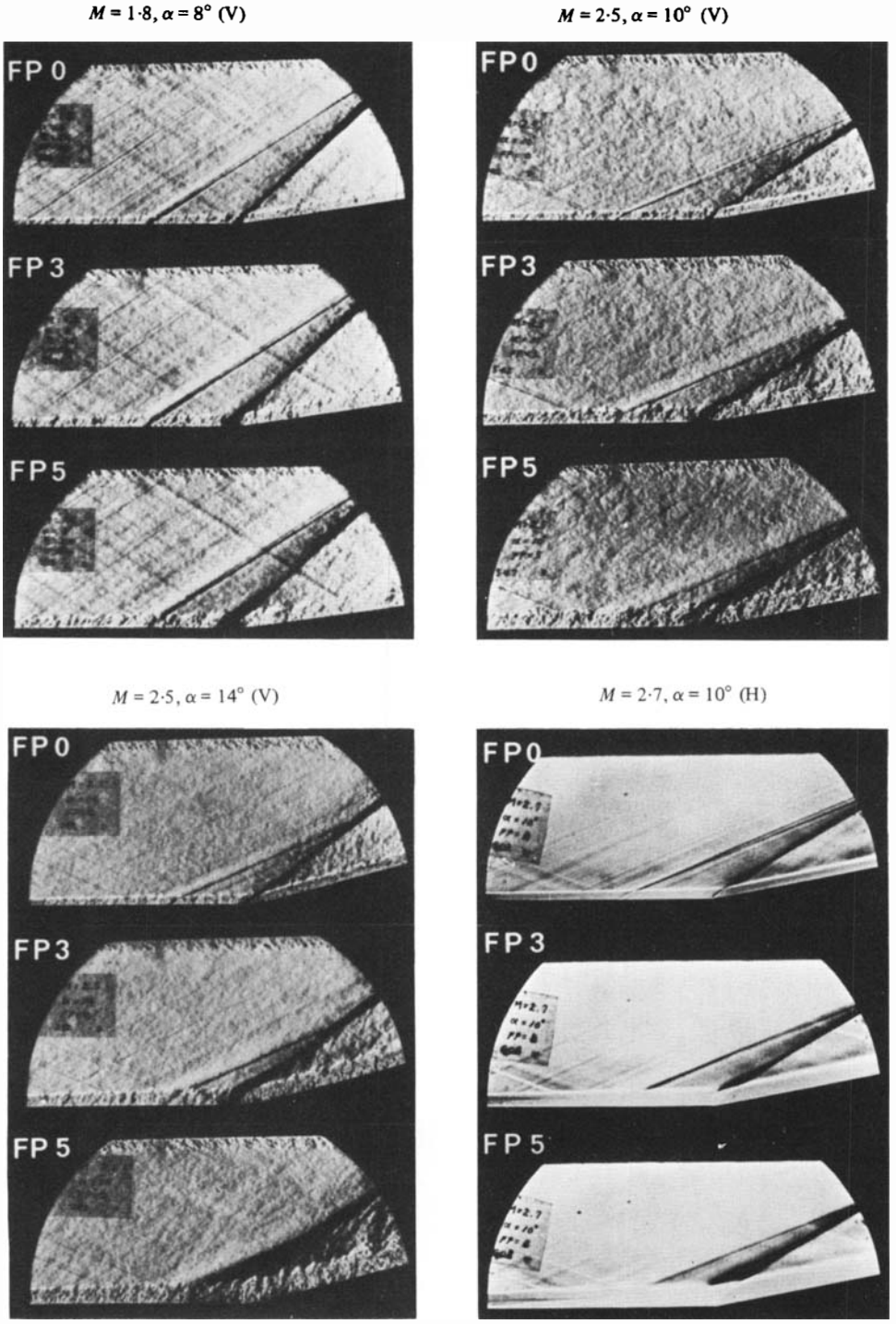

(H) Horizontal cut-off, (V) Vertical cut-off

FIGURE 12. Schlieren photographs.

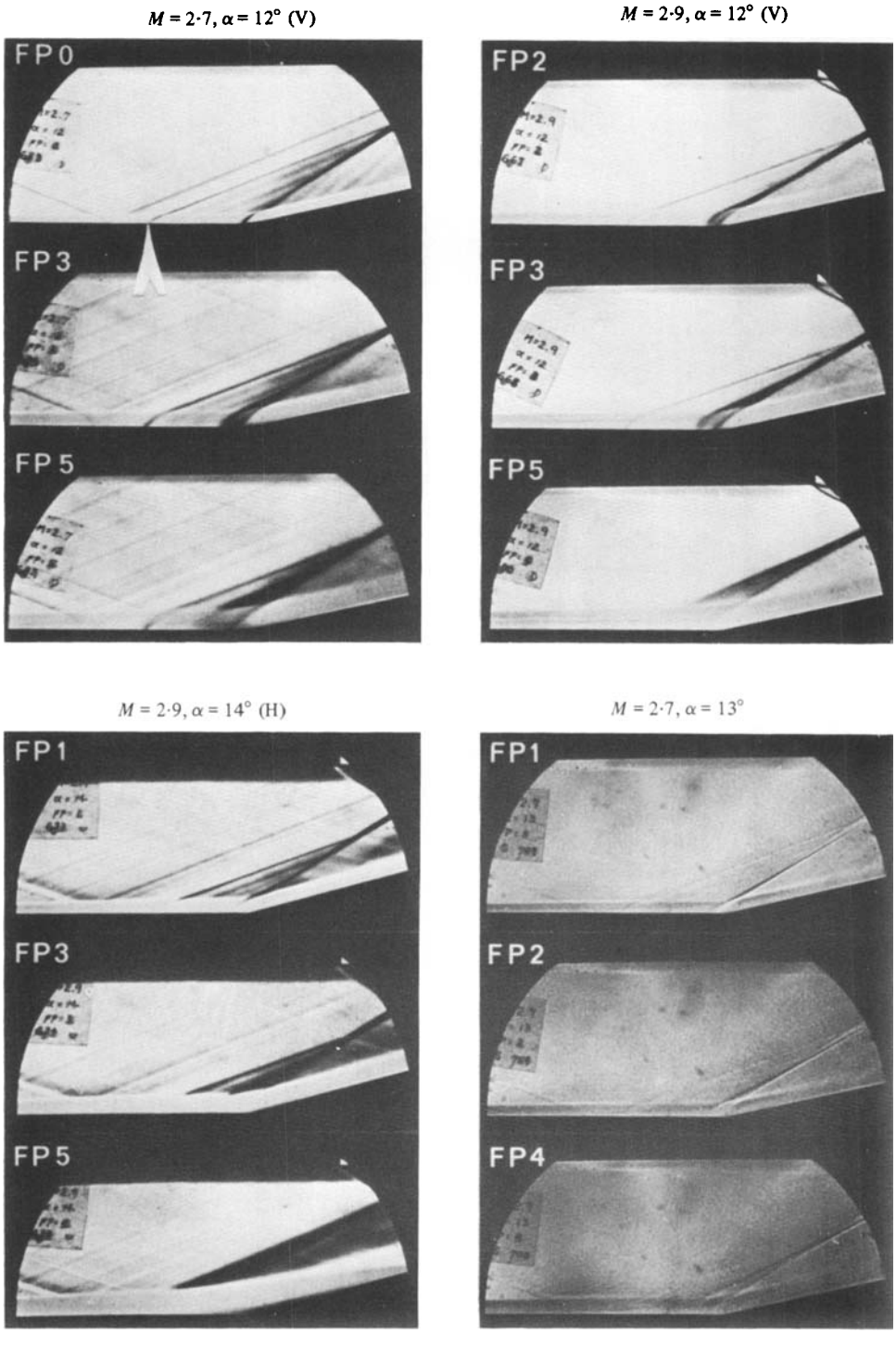

FIGURE 13. Schlieren and shadowgraph photographs.

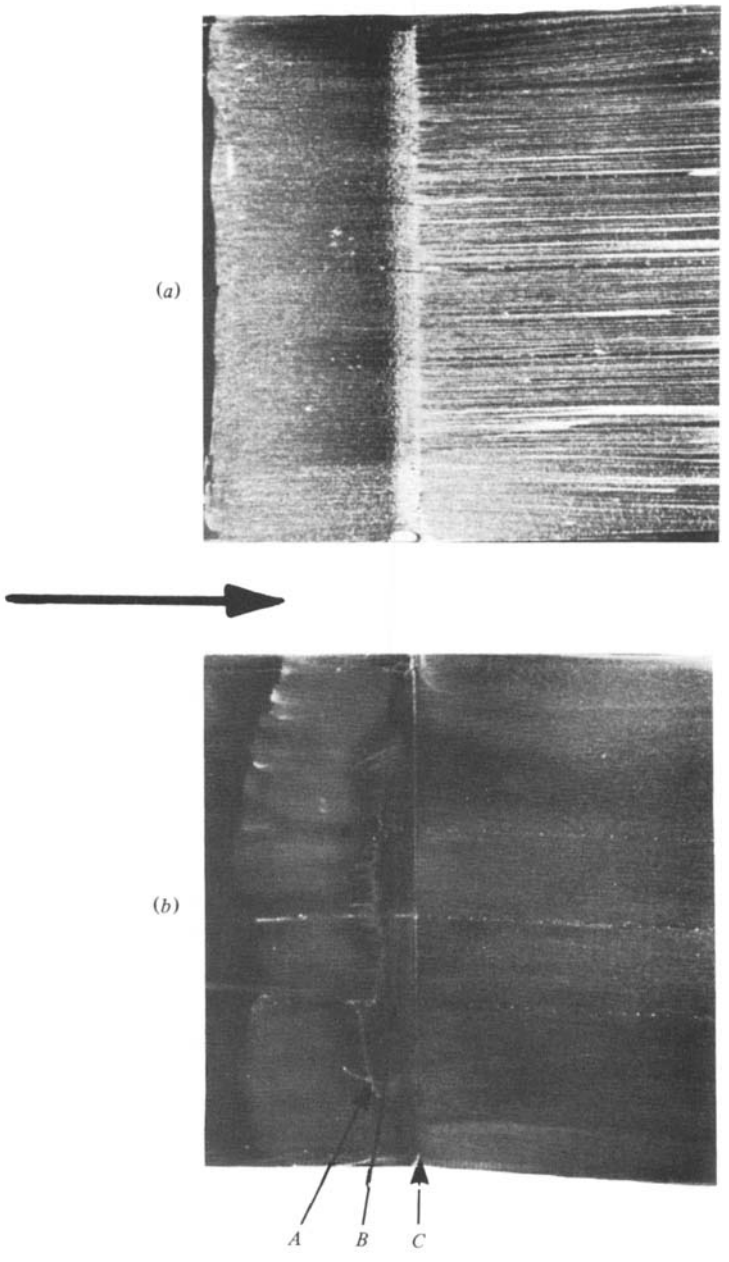

FIGURE 14. Oil-flow photographs. (*a*) $M = 1{\cdot}8$, $\alpha = 8°$, $FP = 3$; (*b*) $M = 2{\cdot}5$, $\alpha = 14°$, $FP = 5$.

of the boundary-layer thickness than those at the lower injection rates. This is because the Mach number gradient in the vertical direction becomes milder and hence a lower Mach number exists over a greater distance from the wall with increasing injection rate.

Some visual observations were made while the tunnel was running to check for the possible instability of the interaction. These were carried out by placing a sheet of

tracing paper over the working section window so that a full size shadowgraph could be projected on it. The shock wave was found to shudder slightly. The amplitude of its oscillation, however, was too small to be measured from a series of spark photographs taken for the same experimental condition.

3.5. *Oil-flow visualization*

Two sample titanium dioxide oil-flow patterns taken at $M = 1{\cdot}8$ with $\alpha = 8°$, $FP = 3$ and at $M = 2{\cdot}5$ with $\alpha = 14°$, $FP = 5$ are shown in figures 14(*a*) and (*b*) respectively. In figure 14(*a*) the oil stagnated at the corner, but the flow was not reversed. The oil pattern shown in figure 14(*b*) is very faint, since much smaller amounts of titanium dioxide pigment had to be used at higher injection rates than at zero injection because of the much-reduced wall shear stress. Note the presence of two accumulation lines upstream of the corner C. It was found from the movement of the oil that the second line B (the one nearer to the corner) was the separation line. The first accumulation line A could well have been produced by the balance between the wall shear stress acting downstream and the pressure forces acting upstream, as discussed by Chapman, Kuehn & Larson (1958). Chapman *et al.* found that the first upstream accumulation line was formed at the position where the pressure rise was $(1{\cdot}3 \pm 0{\cdot}1)\,P_1$. In the present study, the pressure rise was slightly higher; roughly $1{\cdot}57\,P_1$.

As described in §2, another method of oil flow was also used to detect incipient separation. This method involved bleeding a light oil through a pressure tapping upstream of the interaction. The oil ran downstream and, if there was a separation, stopped at the separation line. Occasionally oil left the line of oil at the separation line and droplets were swept downstream. The reattachment position was identified as a formation of oil droplets downstream of the corner, most of which travelled very slowly in the downstream direction. Some of the droplets were seen to be entrained into the separated region, forming streaklines. At each corner angle the injection rate was continuously decreased from the maximum to zero so that the separated region, if present, could be reduced to zero. The injection rate was also gradually raised, starting from a lower rate than that at which incipient separation was found to occur, in order to check for possible hysteresis. No apparent hysteresis was found. This method proved to be quite sensitive, but unfortunately was difficult to photograph, so no results are reproduced here.

4. Discussion

4.1. *Upstream influence*

One of the problems arising in a shock-wave/boundary-layer interaction is that the pressure rise produced by the shock wave propagates upstream through the subsonic part of the boundary layer, and as a result a discontinuous change in pressure, as would occur if the flow were inviscid, cannot be achieved. For the purpose of analysis, the upstream influence, or upstream interaction length Δl, was determined by the method used by Settles & Bogdonoff (1973). They defined it as the distance from the corner position to the intersection of the maximum pressure rise slope with the x-axis (figure 15).

The upstream influence lengths found in the manner described above were normalized by the boundary-layer thickness at the corner position δ_c, which had been

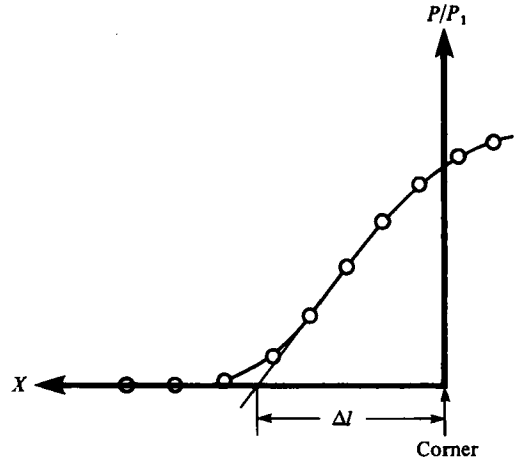

FIGURE 15. Definition of upstream influence length.

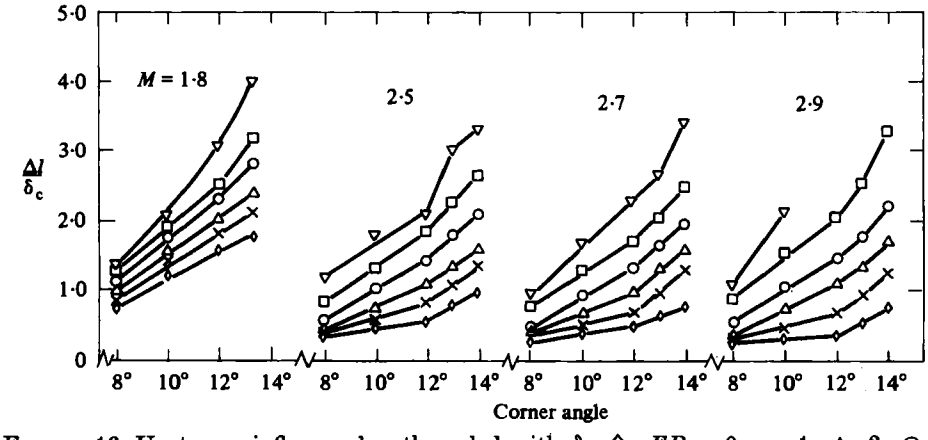

FIGURE 16. Upstream influence length scaled with δ_c. ◇, FP = 0; ×, 1; △, 2; ○, 3; □, 4; ▽, 5. (δ at u/U_e = 0·995.)

measured in the absence of a shock wave at the appropriate injection rate, and are plotted against corner angle for each Mach number in figure 16. It can be seen that the upstream influence length $\Delta l/\delta_c$, increases with increasing injection rate at each corner angle. Thus the increase Δl in upstream influence is more rapid than the increase in boundary-layer thickness produced by the increased injection. Normalizing Δl by the boundary-layer thickness at the start of the interaction would give similar results because δ varies very slowly with x.

In a supersonic flow the upstream transmission of the pressure rise produced by a shock wave must take place through the subsonic part of the boundary layer. Squire & Smith (1980) suggested that the increase in interaction length with increasing injection rate was due to the increase in thickness of the subsonic layer; they demonstrated that a good correlation could be obtained when the interaction length was normalized by the subsonic-layer thickness evaluated at the shock-impingement point and was plotted against peak pressure ratio. The subsonic-layer thicknesses used for this correlation were those measured in the absence of a shock wave.

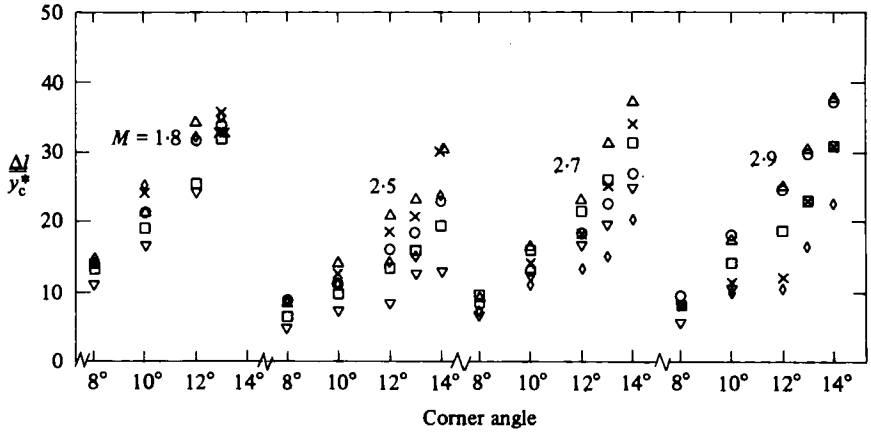

FIGURE 17. Upstream influence length scaled with undisturbed sonic-layer thickness at the corner position. Key as in figure 16.

Under the adiabatic wall condition the sonic point corresponds to $u/U_e \simeq 0{\cdot}64$ at $M = 1{\cdot}8$ and to lower values at higher Mach numbers, reaching $u/U_e \simeq 0{\cdot}51$ at $M = 2{\cdot}9$. Therefore, in the present experiments, where the boundary layer becomes less full with increasing injection rate, the subsonic part of the boundary layer occupies a larger fraction of the boundary-layer thickness at the higher injection rates.

Figure 17 shows the results when the upstream influence length was scaled with the undisturbed subsonic-layer thickness at the corner position that corresponds to the shock-impingement position in Squire & Smith's (1980) correlation. The corner angle was used instead of pressure ratio owing to the absence of peak pressure as found in Squire & Smith's experiments. However, the use of either the pressure ratio at the final downstream position or that at the corner position would give a similar result because, as mentioned in §3.3, these pressures are virtually independent of the injection rate at each corner angle.

Figure 17 shows no systematic variation of the non-dimensional upstream influence length with injection rate, and the results do not collapse onto a single line as found by Squire & Smith. The correlation was no better when the thickness of the sonic layer at the start of the interaction was used to non-dimensionalize the results. An attempt to improve the correlation was made by using various integral parameters, but no success was obtained.

In an extensive study of upstream influence in zero pressure gradient Roshko & Thomke (1976) showed that, for Mach numbers greater than 2·5, a linear relationship existed between the upstream influence length normalized by the boundary-layer thickness ($\Delta l/\delta_1$) at the start of the interaction and the local skin-friction coefficient c_{f_1} at the same point. This linear relation was independent of Mach number and was given by

$$\frac{\Delta l}{\delta_1} = \left(\frac{\alpha}{18{\cdot}29}\right)^{2{\cdot}81}\left\{10^3 c_{f_1} - 1 + \left(\frac{\alpha}{29}\right)^2\right\}, \tag{2}$$

where α is the corner angle in degrees.

The present results for all injection rates at $M = 1{\cdot}8$ and 2·5 are plotted against c_{f_1} in figure 18. It can be seen that, for fixed Mach number and corner angle, the non-

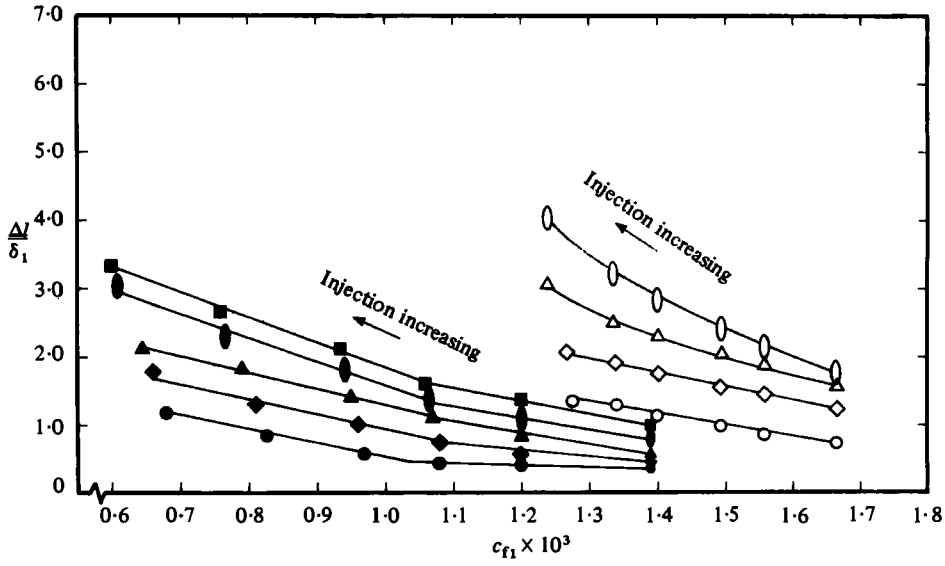

FIGURE 18. Variation of upstream influence length with skin-friction coefficient. ○, $\alpha = 8°$; ◇, 10°; △, 12°; ⬯, 13°; □, 14°; open symbols for $M = 1{\cdot}8$, filled symbols for $M = 2{\cdot}5$. (δ at $u/U_e = 0{\cdot}995$.)

dimensionalized upstream influence length increases with increasing injection rate, i.e. decreasing skin friction, and so is opposite to the trend suggested by (2). Spaid & Frishett (1972) also found that $\Delta l/\delta$ decreased with increasing c_f when the increase in c_f was caused by wall cooling. This confirms the suggestion of Roshko & Thomke that their correlation only holds for flat-plate boundary layers in adiabatic conditions.

The present results for zero injection are compared directly with the Roshko & Thomke correlation in figure 19. In general they lie above the correlation, but they do show an increase in non-dimensional upstream influence with increase in c_f. (It should be noted that Roshko & Thomke use skin-friction coefficients derived from charts based on the van Driest method II as presented by Hopkins (1972); in general these charts give values of c_f that are 0·0001 higher than those derived by Winter & Gaudet (1970), and hence about 0·0002 higher than the measured values. For consistency the present results are plotted against values of c_f derived from the Hopkins charts.) Figure 19 also includes some experimental results from Law (1974), Settles, Bogdonoff & Vas (1976) and Roshko & Thomke (1976) for comparable values of R. As will be seen the results of Settles *et al.* for $M = 2{\cdot}9$ lie very close to the correlation curve, whereas the results of Law at $M = 2{\cdot}9$, which were obtained in similar experimental conditions to the present results, lie above the correlation. Similarly the results of Roshko & Thomke at $M = 2{\cdot}0$ and 2·5 also lie above the correlation. Thus it would appear that the correlation is most valid at Mach numbers above $M = 3$ at relatively high Reynolds numbers.

During the course of this study, it was also found that a good correlation could be obtained by using the pressure-rise ratio attained at the corner position. The boundary-layer equation applied near the wall where the velocity and the flow acceleration are small is

$$\frac{dP}{dx} = \frac{\partial \tau}{\partial y}. \tag{3}$$

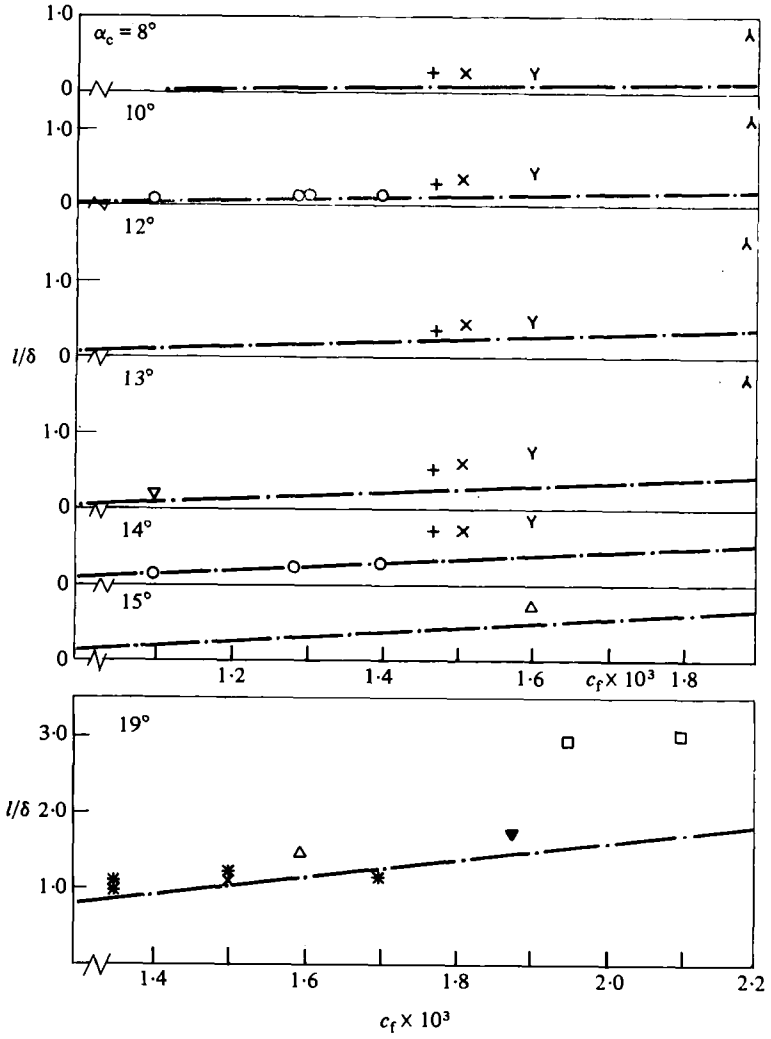

FIGURE 19. Comparison of upstream influence length with correlation of Roshko & Thomke (1976) (— · —). Present results: ⅄, $M = 1{\cdot}8$, $R_\delta = 1{\cdot}9 \times 10^5$; Y, 2·5, $2{\cdot}1 \times 10^5$; ×, 2·7, $2{\cdot}8 \times 10^5$; +, 2·9, $2{\cdot}4 \times 10^5$. Results of Law (1974): △, $M = 2{\cdot}96$, $R_\delta = 1{\cdot}4 \times 10^5$. Results of Settles *et al.* (1976): ○, $M = 2{\cdot}9$, $R_\delta = 5$–50×10^5. Results of Roshko & Thomke (1976): ▽, $M = 3{\cdot}96$, $R_\delta = 3{\cdot}8 \times 10^5$; ✱, 2·98, 1–$3{\cdot}8 \times 10^5$; ▼, 2·49, 1×10^5; □, 2·0, 1–2×10^5. (δ at $u/U_e = 0{\cdot}995$.)

By applying order-of-magnitude considerations to (3) and following the analysis of Chapman *et al.* (1958) by taking the wall shear stress at the beginning of the interaction as a measure of the shear stress, the following relation can be obtained:

$$\frac{P_c - P_1}{\Delta l} \propto \frac{\tau_{w1}}{\delta_1}. \tag{4}$$

After dividing both sides by $\frac{1}{2}\gamma p_1 M_{e1}^2$ this gives

$$\frac{\Delta l}{\delta_1} \propto \left(\frac{P_c}{P_1} - 1\right) \Big/ c_{f_1} M_{e1}^2, \tag{5}$$

where M_{e1} is the freestream Mach number at the start of the interaction.

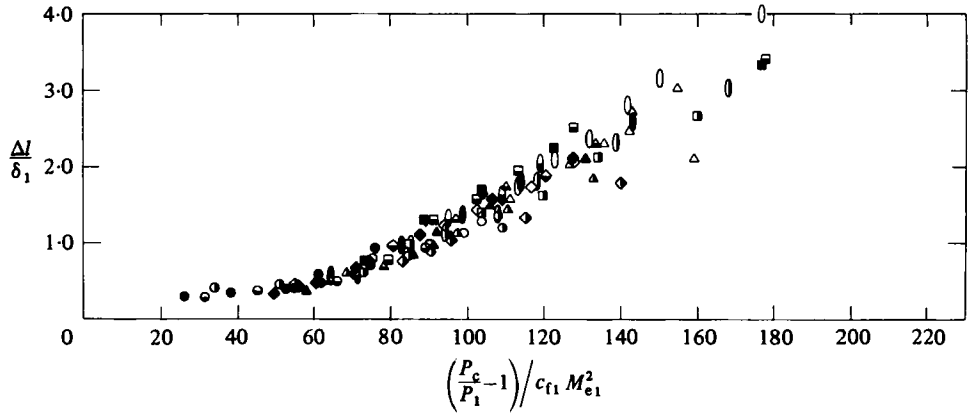

FIGURE 20. Correlation of upstream influence length with corner pressure. Present results: ○, $\alpha = 8°$; ◇, 10°; △, 12°; ⬯, 13°; □, 14°; open symbols, $M = 1{\cdot}8$; half-filled vertical symbols, $M = 2{\cdot}5$; half-filled horizontal symbols, $M = 2{\cdot}7$; filled symbols, $M = 2{\cdot}9$. (δ at $u/U_e = 0{\cdot}995$.)

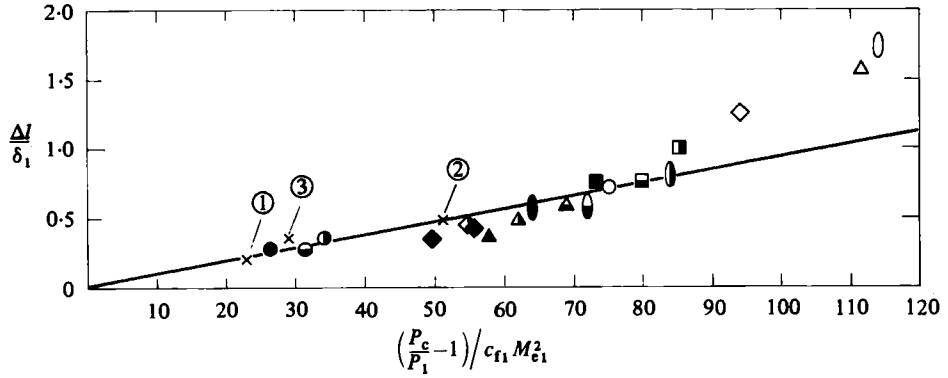

FIGURE 21. Correlation of upstream influence length with corner pressure for zero injection. Present results as in figure 20. Results of Roshko & Thomke (1976): ①, $\alpha = 13°$; ②, $\alpha = 19°$ ($M = 3{\cdot}96$). Results of Spaid & Frishett (1972): ③, $\alpha = 12{\cdot}6°$ ($M = 2{\cdot}93$). (δ at $u/U_e = 0{\cdot}995$.)

Figure 20 shows the upstream-influence results plotted in the co-ordinate system suggested by (5). It can be seen that a reasonably good correlation is obtained for all Mach numbers, corner angles and injection rates investigated. The scatter and the deviation from the linear relation implied by (5) may be due to the inclusion of separated-flow data. Figure 21 shows only the zero-injection results. As can be seen the results lie close to a straight line given by

$$\frac{\Delta l}{\delta_1} = 9{\cdot}5 \times 10^{-3}\left(\frac{P_c}{P_1}-1\right)\Big/c_{f1}M_{e1}^2. \tag{6}$$

Figures 20 and 21 indicate that the upstream influence only approaches zero as P_c/P_1 tends to unity, which means the corner angle is tending to zero. Thus there is an upstream influence whenever there is a disturbance in the flow.

Also shown in figure 21 are some of the results from the experiments of Roshko & Thomke (1976) and of Spaid & Frishett (1972). As will be seen they also fall on the correlation. Unfortunately, results from other experiments for other Reynolds

numbers could not be examined owing to the non-availability of corner pressure or skin-friction data.

One drawback of the present correlation is that a corner pressure is not known in advance. However, if the correlation shown in figures 10 or 11 were to be found for other conditions, the corner pressure could be estimated from a corner angle. Alternatively the corner pressure at high Mach numbers could be found by the integral method recently developed by Rosen, Roshko & Pavish (1980).

4.2. *Incipient separation*

An important parameter for a designer is the pressure rise, or corner angle, that just produces separation, since this condition marks the safe limit of orderly flow beyond which unpredictable changes in the *overall* flow field may occur. This first appearance of a region of reversed flow adjacent to the wall is referred to as incipient separation. For two-dimensional flow it is defined as the condition where the wall shear stress at one point is precisely zero, but is positive everywhere else. This definition is straightforward, but experimental detection of this condition is difficult. It is well known that the results obtained depend critically on the method used to find it.

The wall shear stress can of course be measured directly by using a skin-friction meter. The equipment, however, is costly and difficult to use, since the detection of incipient separation involves measurements of extremely small values of skin friction in the region of a very steep pressure gradient. Thus a number of different alternative methods or criteria have been used to detect incipient separation.

In the present study an attempt to determine the conditions for incipient separation was made by using the following six methods:

(1) surface oil-flow visualization;

(2) the first appearance of a 'kink' or triple inflection point in the surface-pressure distributions (Kuehn 1959);

(3) a break, or inflection, in the variation of pressure at, or near, the corner when plotted against corner angle (Roshko & Thomke 1969);

(4) the change of the flow-turning system from a single-wedge compression to a double-wedge compression process (Spaid & Frishett 1972; Settles & Bogdonoff 1973);

(5) extrapolation of separation lengths, as determined by extrapolating the separation shock to the wall, to zero (Spaid & Frishett 1972; Appels & Richards 1975); and

(6) a break in the variation of upstream-influence length when plotted against corner angle (Kessler, Reilly & Mockapetris 1970; Settles & Bogdonoff 1973).

In fact the last four methods did not give any clear indication of separation in the present study, and so the discussion which follows is based on results obtained by the inflection-point and oil-bleed methods, with some support from patterns obtained by use of titanium oxide. A typical set of results for one Mach number ($M = 2{\cdot}9$) is presented in figure 22, where the results for incipient separation are plotted against the nominal blowing parameter FP. Although this method of presentation is rather artificial, it is useful in understanding the significance of the results and the methods by which they were obtained. For example, with the wedge at 13° the pressure distributions at zero injection and with the lowest injection rate did not show inflection points, whereas all the pressure distributions at higher injection rates did show inflection points. Thus incipient separation is assumed to occur just above the lowest

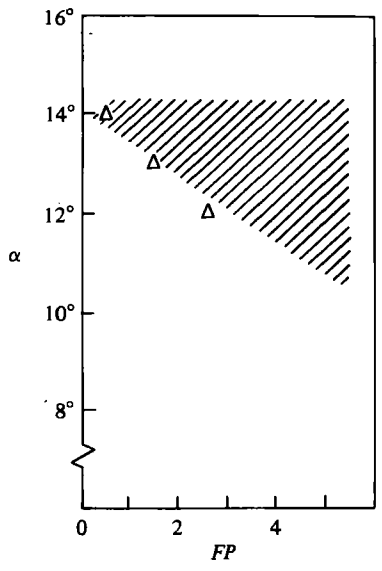

FIGURE 22.

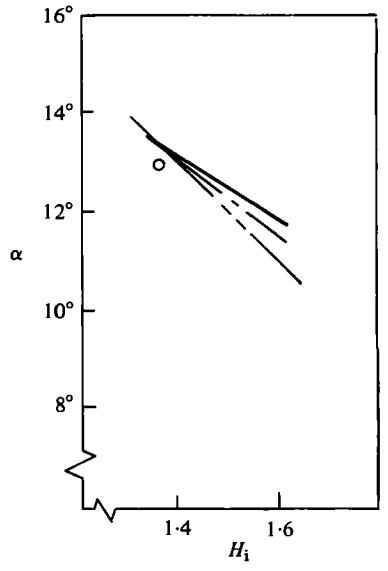

FIGURE 23.

FIGURE 22. Corner angles for incipient separation at $M = 2{\cdot}9$. △, as indicated by inflection methods; ///, separation shown by oil-bleed method.

FIGURE 23. Variation of corner angles for incipient separation with H_1. ○, $M = 1{\cdot}8$; ——, 2·5; — — —, 2·7; — — — —, 2·9.

blowing rate as shown by the triangular point in figure 22. At the same wedge angle the oil-bleed method showed a clear separation and reattachment at the higher injection rates, but the separated region became smaller as the injection rate was reduced, and eventually disappeared just below the rate corresponding to $FP = 2$. As will be seen, the conditions for incipient separation as predicted by the oil-bleed and inflection-point methods are in close agreement, and similar agreement was found at other Mach numbers. This appears to contradict the findings of other workers who have suggested that the inflection-point method is a less-sensitive method for detecting separation than the oil-flow method. However, it may be that in the present experiment the close spacing of the pressure holes has made the detection of the inflection point easier. In general, the results obtained from the surface oil flow using titanium dioxide confirmed the oil-bleed results. For example, on the wedge at 14° at $M = 2{\cdot}5$ the surface oil flow showed clear lines of separation and attachment for injection rates corresponding to $FP = 3$ and above (see figure 14*b*), and possible signs of separation at lower injection rates, while the oil-bleed method gave clear indications of separation at zero injection.

The results for all the test Mach numbers as found by the oil-bleed method are plotted in figure 23 against the value of H_1 at the start of the interaction in the absence of the shock, but at the appropriate injection rate. Notice that in the figure the results for $M = 1{\cdot}8$ are only represented by a single point, since at this Mach number incipient separation was only observed on the wedge at 13°, the highest angle tested. As will be seen, the corner angles for incipient separation at all Mach numbers collapse onto a narrow band when plotted in this way. The figure shows a significant fall in corner angle for incipient separation with increase in H_1.

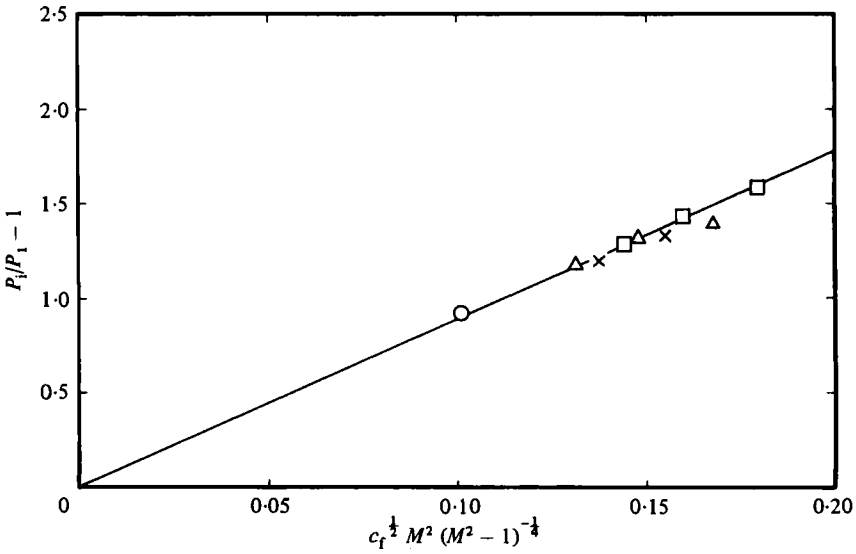

FIGURE 24. Variation of pressure rise for incipient separation with skin-friction coefficient. ○, M = 1·8; ×, 2·5; △, 2·7; □, 2·9.

The conditions for incipient separation were also plotted against other boundary-layer parameters, and it was found that at each Mach number the overall pressure rise at incipient separation was directly proportional to the square root of the skin-friction coefficient at the start of the interaction in the absence of the shock but at the appropriate injection rate. Furthermore, it was found that the results for all the test Mach numbers collapsed onto a single line when plotted against $c_f^{\frac{1}{2}} M^2(M^2-1)^{-\frac{1}{4}}$ (figure 24). This form of plotting was suggested by the work of Popinski & Ehrlich (1966), who deduced this form of dependence for the conditions for incipient separation at compression corners for upstream boundary layers growing in zero-pressure-gradient conditions. More recent work (Elfstrom 1972) has shown that at high Reynolds numbers the conditions for incipient separation are almost independent of Reynolds number, that is they do not vary directly with $c_f^{\frac{1}{2}}$. Thus the present results should not be taken as confirming the earlier analysis of Popinski & Ehrlich, but rather that, at a particular Reynolds number, the effect of the state of the upstream boundary layer on incipient separation is proportional to the square root of the skin-friction coefficient.

5. Conclusions

The present tests show that by using injection through a porous surface upstream of a compression corner it is possible to produce a wide range of boundary-layer profiles ahead of the shock interaction at the corner. The static pressure distributions and the surface oil-flow patterns indicate that the two-dimensionality of the flow is satisfactory.

The main features of the results are (i) the large increase in the scale of the interaction, and in particular the upstream-influence length, with decreasing fullness of the upstream velocity profile, and (ii) the apparent independence of the pressure at

the corner with the shape of the approaching boundary layer. In general the present results with zero injection are in agreement with results from other sources.

The results also show that the corner angle for incipient separation falls as the profile of the approaching boundary layer becomes less full, and that, within the range of conditions for the present tests, the overall pressure rise for incipient separation is directly proportional to the square root of the skin-friction coefficient of the undisturbed boundary layer.

REFERENCES

Appels, C. & Richards, B. E. 1975 Incipient separation of a compressible turbulent boundary layer. *AGARD CP*-168, Paper no. 21.

Bradshaw, P. & Unsworth, K. 1973 A note on Preston tube calibration in compressible flow. *Imperial College, London, Rep. Aero.* no. 73-07.

Chew, Y. T. & Squire, L. C. 1979 The boundary layer development downstream of a shock interaction at an expansion corner. *Aero. Res. Counc. R. & M.* no. 3839.

Chapman, D. R., Kuehn, D. M. & Larson, H. K. 1958 Investigation of separated flows in supersonic and subsonic streams with emphasis on the effect of transition. *NACA Rep.* no. 1356.

van Driest, E. R. 1951 Turbulent boundary layer in compressible fluids. *J. Aero. Sci.* **18**, 145.

Elfstrom, G. M. 1972 Turbulent hypersonic turbulent flow at a wedge compression corner. *J. Fluid Mech.* **53**, 113.

Hopkins, E. J. 1972 Charts for predicting turbulent skin friction from the van Driest method (II). *NACA TN* D-6945.

Hunter, L. G. & Reekes, B. L. 1971 Results of a strong interaction, wakelike model of separated and reattaching turbulent flows. *A.I.A.A. J.* **9**, 703.

Jeromin, L. O. F. 1966 An experimental investigation of compressible turbulent boundary layers with air injection. *Aero. Res. Counc. R. & M.* no. 3526.

Kessler, W. C., Reilly, J. F. & Mockapetris, L. J. 1970 Supersonic turbulent boundary layer interaction with an expansion ramp and a compression corner. *McDonell–Douglas Rep.* MDCE0264.

Kuehn, D. M. 1959 Experimental investigation of the pressure rise required for the incipient separation of turbulent boundary layers in two-dimensional supersonic flow. *NACA Memo* 1-21-59A (*NACA*/TIL/6209).

Law, C. H. 1974 Supersonic, turbulent boundary-layer separation. *A.I.A.A. J.* **12**, 794.

Maltby, R. L. 1962 Flow visualization in wind tunnels using indicators. *AGARDograph* no. 70.

Popinski, Z. & Ehrlich, C. F. 1966 Development design method for predicting hypersonic aerodynamic control characteristics. *U.S.A.F. Tech. Rep.* AFFDL-TR-66-85, *Wright Patterson A.F.B.*

Roshko, A. & Thomke, G. J. 1969 Supersonic, turbulent boundary-layer interaction with a compression corner at very high Reynolds number. In *Proc. Symp. on viscous Interaction Phenomena in Supersonic and Hypersonic Flow, Wright Patterson A.F.B., Ohio*, p. 109. University of Dayton Press.

Roshko, A. & Thomke, G. J. 1976 Flare-induced interaction lengths in supersonic, turbulent boundary layers. *A.I.A.A. J.* **14**, 873.

Rosen, R., Roshko, A. & Pavish, D. L. 1980 A two-layer calculation for the initial interaction region of an unseparated supersonic turbulent boundary layer with a ramp. *A.I.A.A. Paper* no. 80-0135.

Settles, G. S. & Bogdonoff, S. M. 1973 Separation of a supersonic turbulent boundary layer at moderate to high Reynolds numbers. *A.I.A.A. Paper* no. 73-666.

Settles, G. S., Bogdonoff, S. M. & Vas, I. E. 1976 Incipient separation of a supersonic turbulent boundary layer at high Reynolds numbers. *A.I.A.A. J.* **14**, 50.

Smith, M. J. 1977 Interaction of a shock-wave with a boundary layer disturbed by injection. Ph.D. dissertation, Cambridge University.

SPAID, F. W. & FRISHETT, J. C. 1972 Incipient separation of a supersonic, turbulent boundary layer, including effects of heat transfer. *A.I.A.A. J.* **10**, 915.

SPALDING, D. B. & CHI, S. W. 1964 The drag of a compressible boundary layer on a smooth flat plate with and without heat transfer. *J. Fluid Mech.* **18**, 117.

SQUIRE, L. C. & SMITH, M. J. 1980 Interaction of a shock wave with a boundary layer disturbed by injection. *Aero. Q.* **31**, 85.

WINTER, K. G. & GAUDET, L. 1970 Turbulent boundary-layer studies at high Reynolds numbers at Mach numbers between 0·2 and 2·8. *Aero. Res. Counc. R. & M.* no. 3712.